Algorithm Optimization for Rockfalls Alarm System Based on Fiber Polarization Sensing

Algorithm Optimization for Rockfalls Alarm System Based on Fiber Polarization Sensing

Saverio Pellegrini, Giuseppe Rizzelli, Marco Barla, and Roberto Gaudino, *Senior Member, IEEE*.

***Abstract*—The mountain scenario is often subject to catastrophic events such as rockfalls and avalanches, potentially dangerous for both people and civil infrastructures. Early-warning alarm systems that in case of such events can immediately turn on a traffic light on a mountain road and send remote alarms to control rooms, have already been developed in the geotechnical engineering sector, but all have some limitations and/or very high costs. In this work we propose an immediate-warning monitoring system based on fiber polarization sensing. Anomalies such as rockfalls and avalanches would change the instantaneous birefringence of the fiber installed in the area to be monitored, and can be sensed by looking at the state of polarization at the fiber output. The novelty of our paper is the development of an algorithm that is able to detect dangerous events, which we experimentally emulated on a reduced scale physical model of a mountain slope, in which fibers have been buried in different configurations. Our findings show that the system can correctly sense all the experimentally generated rockfall phenomena and for all the installed fiber configurations, and it is also robust to false alarms, provided that the monitoring algorithm main parameters are properly set.**

***Index Terms*—Optical fibers, polarization, birefringence, rockfalls, monitoring and alarm system.**

I. Introduction

THE use of optical fibers as sensing devices is not a recent idea [1]. Over the years it has been found that they are very suitable as sensors in many different scenarios, including chemical and mechanical applications, or even to sense temperature variations. This flexibility is beneficial to the geotechnical field, where modern monitoring techniques can be enhanced using fiber based systems [2]. Optical sensing techniques can be divided in two main classes:

a) **Distributed sensing [3]**: this is the best solution in terms of performances. The whole fiber length can act as a sensor and anomalies can be detected and localized with high spatial resolution, ranging from cm to m. The drawbacks are typically the complexity of the systems and the high cost, due to the need of very sophisticated interrogators. Moreover, most of these systems are very slow, requiring up to several minutes for a full acquisition, thus they are not suitable for real-time fast alarm.

b) **Discrete sensing [4] [5]**: this solution is based on the installation of a high number of sensors, tipically fiber Bragg gratings, along the fiber profile. Anomalies (external events inducing stresses on the fiber) can be localized, but discretely in space, with resolution depending on the number of sensors employed. Because of the high number of sensors needed to have an appropriate spatial resolution, this is usually again a high cost solution.

Interferometric techniques can also be used to increase the event localization capability at a reduced cost [6]–[8]. In this work, we focus on the monitoring and immediate alarm generation in the mountain scenario, often subject to hazardous events that can damage roads or entire areas and harm lives [9], [10]. In particular, to monitor these events, we propose to sense the mechanical and vibrational stresses induced on the fiber by the surrounding terrain, that can be detected through a monitoring system based on underground fibers buried in situ. More specifically, since mechanical stresses (in our case mainly shear stresses, caused by falling rock masses [11]) induced on the fiber during our experiments will instantaneously change the birefringence, we measure the state of polarization at the fiber output. We point out that, focusing on the goal of fast alarm generation after a catastrophic event, distributed sensing with high spatial resolution is not strictly needed, but it is anyway required that vibrations are sensed in any position along the deployed fiber, as it actually happens when monitoring fiber polarization. The aim of this work is to characterize and study an optical fiber-based monitoring system, with the requirements of reliability, simplicity, improved performances with respect to current solutions and, above all, lower cost than a state of the art system.

Polarization sensing is obviously not a new idea, but in this work the novelty is in the following:

1) achievement of immediate alarm generation, with delay times in the order of one second. The typical application we have in mind is an alarm system in the mountain area that can for instance turn red a traffic light on a mountain road immediately after a rockfall or an avalanche. Clearly, speed of detection is a key element.
2) development of an algorithm for state of polarization detection. We optimize its parameter and validate it on an experimental small scale physical model.

In the geotechnical and mountain engineering fields, a high number of (not optical) monitoring techniques have already been developed and installed [12], [13] concerning, for example, tracking of initiation mechanisms, the very first signs that some hazardous event could be about to manifest. Other methods are used to monitor the debris flow dynamics, that is to measure vibrations caused by the flowing mass, sense

S. Pellegrini and R. Gaudino are with Dipartimento di Elettronica e Telecomunicazioni (DET), Politecnico di Torino, Italy (e-mail: saverio.pellegrini@polito.it; roberto.gaudino@polito.it).

G. Rizzelli is with LINKS Foundation, Torino, Italy (e-mail: giuseppe.rizzelli@linksfoundation.com).

M. Barla is with Department of Structural, Geotechnical and Building Engineering (DISEG), Politecnico di Torino, Italy (e-mail: marco.barla@polito.it).

This article has been accepted for publication in IEEE Photonics Journal. This is the author's version which has not been fully edited and
content may change prior to final publication. Citation information: DOI 10.1109/JPHOT.2023.3281670

flow depth, basal stress or record surface flow velocity. The existing geotechnical solutions are typically affected by one or more of the following drawbacks:

- Low reliability: the monitoring system should be located in positions where the acquired data are safe to be interpreted correctly. Unreliable data evaluations would increase false and missed alarms occurrences, when detecting dangerous events.
- Coverage: monitoring is usually active over areas of limited extent, which could cause the system to miss dangerous events occurring in areas out of reach.
- Maintenance: the sensors installed need maintenance to be always fully operative. This represents a problem, since they are often difficult to reach.
- Real-time requirements: its not always possible to have a real-time prediction of dangerous events. Usually, some of the existing monitoring systems have a quite long acquisition time (of the order of a few minutes).
- For the specific target of our investigation, it is important for the in situ sensing devices to be inexpensive, since they might be damaged by catastrophic events.

Existing fiber optics sensing techniques can solve or at least mitigate the majority of these problems, at the expense of increased cost and complexity. The best performing state of the art solutions are mainly distributed sensing techniques [14] based on Rayleigh, Raman and Brillouin scattering. Moreover, sensing is enabled on vibrations, strain and temperature, over distances up to few hundred km [15], and with spatial resolutions down to few centimeters (or even less) along the cable which, for geotechnical applications, represents an enormous advantage [16] [17], despite the high cost. On the contrary, our proposed monitoring system can be classified as "quasi distributed" since it can monitor events occurring in any position along the fiber (and not only in some positions as in discrete sensing solutions), but without the spatial resolution that distributed sensing can provide. This approach enables the monitoring of large geographical areas, but does not allow to locate events in space. It is anyway perfectly suitable for situations in which an alarm signal should be switched on, when strong and anomalous vibrations are detected in any position along the fiber length. Moreover, this solution does not need costly equipment or complex signal processing and, unlike current monitoring solutions in the geotechnical sector, can in principle have the interrogator placed 10-20 km away from the actual monitoring site, where a few hundred meters of fiber would be buried.

The system we propose in this manuscript is based on the monitoring of optical polarization [18]. The state of polarization (SOP) of light propagating inside an optical fiber can be uniquely described in a three dimensional space by the Stokes vector ($\vec{S}$), identified by the three Stokes parameters, S_1, S_2, S_3. S_0 is not considered, since it represents the power at the fiber output, which is constant and does not carry any information. The three dimensional space over which $\vec{S}$ is identified, is the Poincaré sphere [19]. If external stresses are applied to the fiber, the birefringence [20]–[22] changes, resulting in the angular variation of the $\vec{S}$ vector in the Poincaré space. This variation can be detected by monitoring the SOP angular speed, the angular variation over time of the Stokes vector: we call this parameter state of polarization angular speed (SOPAS).

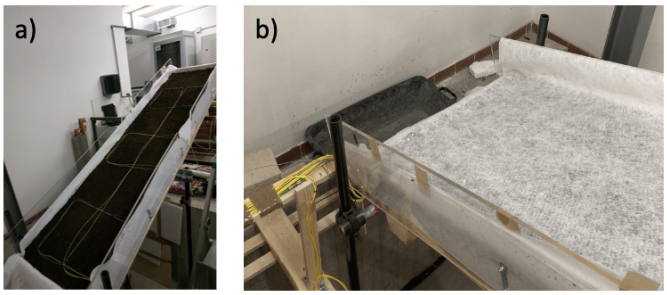

Fig. 1. a) Experimental model with no geotextile showing the most superficial (and not yet buried) fiber configuration, b) slide covered in geotextile.

In the following Sections we will present a possible implementation and the related post-processing algorithms for a fiber based alarm system relying on detecting anomalous polarization variations, and then we will show our experimental demonstration based on a reduced scale model of the slope of a mountain (Fig. 1), on which events emulating real rockfalls were generated. We have developed a post-processing and a real-time algorithm (implemented through Matlab) able to compute the SOPAS and, using a proper algorithm, detect if SOPAS anomalous variations take place over time.

The reminder of this manuscript is organized as follows: in Section II, the experimental setup used for the experiments is presented and explained in details, and in Section III the working principle of the detection algorithm is presented. Section IV reports the experimental demonstrator results including discussion on a true real-time implementation. A discussion is given in Section V, and conclusions in Section VI.

II. Experimental setup of the polarization-based alarm-generating system

Our proposal is based on the experimental setup shown in Fig. 2: the laser emits a linearly polarized continuous-wave (CW) optical signal with 0 dBm optical power to the in-situ fiber deployed underground, in the area to be monitored (e.g. a mountain gully), which in our case is the model in Fig. 1. The output end of the fiber is connected to a polarimeter, a commercial instrument that allows to measure the Stokes parameters with a sampling frequency f_s. A PC then extracts the SOP samples from the polarimeter to process them according to the algorithm that will be described in the next Sect. III, and thus monitors the SOPAS time-evolution. The algorithm is developed to produce an alarm (e.g. a traffic light turning red or a remotely transmitted hazards alarm in a real-time scenario) if some anomaly is detected. The optical source used in our experiments is a low cost (a few hundred euros) Fabry-Perot (FP) laser emitting light at 1550 nm. Light then propagates inside a single mode fiber (SMF), buried within the soil of the monitoring site model. The monitoring site recreated in our lab is a scale model of the slope of a mountain [23] (Fig. 1). Essentially, it is a ramp made of

This article has been accepted for publication in IEEE Photonics Journal. This is the author's version which has not been fully edited and content may change prior to final publication. Citation information: DOI 10.1109/JPHOT.2023.3281670

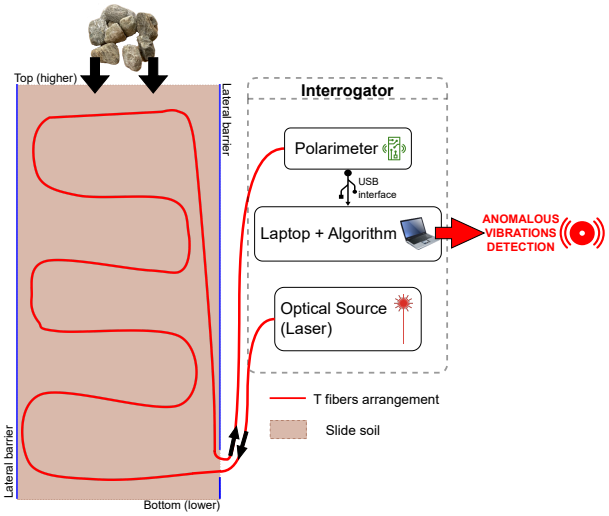

Fig. 2. Scheme of the monitoring system showing the T (red line) fiber configuration. The same configuration exists at different depths.

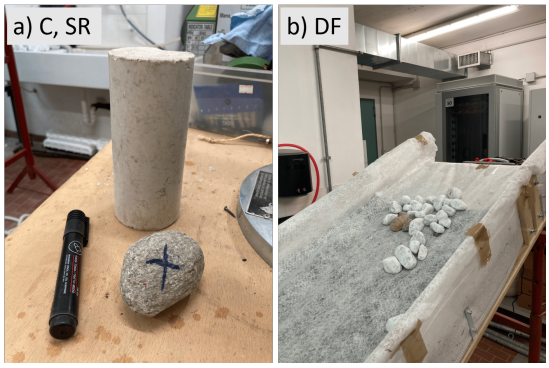

Fig. 3. a) Picture of the cylinder and the single rock used to generate C and SR events. b) Example of rockfalls event occurring on the slide.

wood inclined by 30°, 0.7 meters wide and about 3 meters long. It has been filled with a mixture of sand and soil for a total thickness of about 10 cm. A total of three optical fibers have been deployed inside the soil at three different depths (1, 5 and 9 cm). The focus of this work is on the "transversal" (T) configuration, coloured in red in Fig. 2. The T fibers are installed in a serpentine layout, with six transversal crossings of the slope longitudinal section. We conducted several experiments also on other configurations installed longitudinally along the model, but we observed no significant differences and therefore we will not show them here. The soil and sand mixtures is enclosed within a layer of geotextile material (see Fig. 1b), to prevent it from being eroded by the repeated rockfalls. To distinguish fibers of the same kind buried at different depths, a convention has been adopted: number "1" indicates the deepest at 9 cm from the surface, number "2" refers to the middle one at 5 cm, and number "3" is for the most superficial, at 1 cm depth. For instance, T1 is used to name the fiber installed at the larger depth (9 cm) with a T configuration. Three different types of mechanical stresses have been generated over the slope in order to emulate real, possibly dangerous, rockfall events:

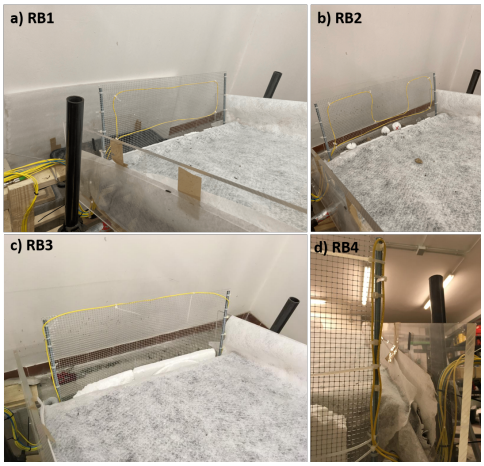

Fig. 4. Pictures of the four rockfall barrier configurations. a) RB1: single loop, b) RB2: double loop, c) RB3: fiber on the perimeter, d) RB4: fiber on one support.

- Single rock (SR): rolling of a 270 grams single rock as in Fig. 3a.
- Cylinder (C): rolling of a 890 grams test cylinder made of ceramic material, 15 cm long and with a diameter of 5 cm (see Fig. 3a).
- Rockfall (RF): rolling of 25 rocks about 5 cm wide, each weighting 280 grams on average, as shown in Fig. 3b.

A high number of SOPAS traces have been acquired, by generating many repetitions of the aforementioned events. Moreover, we performed several measurements of the "steady" condition, i.e. without any rockfall event: this "background noise" on SOP time evolution was important to study the occurrences of false alarms, as we will discuss in the following. At the bottom of the slope, we also built a scale reproduction of a rockfall metallic barrier [24], [25], over which different fibers layouts have been arranged, as shown in Fig. 4. These configurations have been selected in order to test which part of the barrier could be the most sensible to rockfalls, by placing the fiber on the perimeter of the grid (Fig. 4c), in the center (Fig. 4a and 4b) or on a support (Fig. 4d).

The polarimeter used to perform our tests is the Novoptel PM1000, equipped with a photodetector covering an extended C-band in the 1501-1565 nm range, analog bandwidth of 25 MHz and acceptable input optical power in the range from -36 dBm to +4 dBm. This device is connected by a USB cable to a computer where, through a Matlab script or the device GUI, hardware parameters such as the sampling frequency f_s or the total acquisition time t_{tot} can be set. The polarimeter registers can be queried to extract the Stokes parameters samples.

III. SOPAS ALGORITHM FOR ANOMALOUS VIBRATIONS DETECTION

The block diagram of the algorithm developed to process the SOP samples and generate alarms when anomalous conditions are detected is shown in Fig. 5. The polarimeter is the source of the Stokes parameters samples taken at discrete time instants k ($S_1[k]$, $S_2[k]$, $S_3[k]$). Unless otherwise specified, all the results in this work have been obtained by first acquiring SOP samples

This article has been accepted for publication in IEEE Photonics Journal. This is the author's version which has not been fully edited and content may change prior to final publication. Citation information: DOI 10.1109/JPHOT.2023.3281670

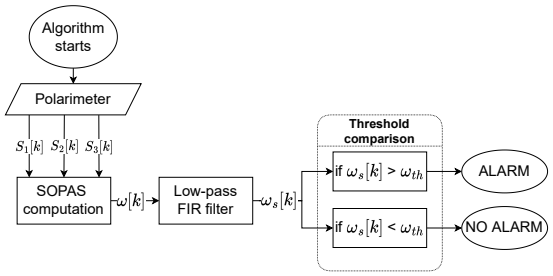

Fig. 5. Algorithm used for SOP processing and alarm generation. $S_1[k]$, $S_2[k]$, $S_3[k]$ are the three Stokes parameters considered at discrete time k. $\omega[k]$ represents the SOPAS sample, $\omega_s[k]$ is its filtered version. ω_{th} is the threshold each $\omega_s[k]$ sample is compared to.

for t_{tot} seconds, and then elaborating the whole acquisition through Matlab, in post-processing. The results of some tests using the polarimeter as real-time source will also be shown: in this case SOP samples are extracted from the device registers at every instant. In our first experiments we chose $f_s = 48.83$ kHz and a total acquisition time $t_{tot} = 21.5$ seconds. The second block computes the SOPAS by applying Equation 1 to each sample, where $\omega[k]$ is the discrete SOPAS, T_s is the sampling period and $(\vec{S}^k, \vec{S}^{k-1})$ is the dot product between the Stokes vectors at time k and at time $k-1$. The idea followed to compute the angular speed is similar to the calculation of the derivative of the angle in discrete time.

$$\omega[k] = \left| \arccos \left(\frac{(\vec{S}^k, \vec{S}^{k-1})}{\left\|\vec{S}^k\right\| \left\|\vec{S}^{k-1}\right\|} \right) \right| \cdot \frac{1}{T_s} \qquad (1)$$

Using the angular speed to detect anomalies occurring on the fiber allows to reduce a three dimensional problem into one dimension, much easier to manage. In particular, the mechanical stresses occurring on the fiber can be easily observed through the SOPAS, since birefringence variations along the fiber induce abrupt changes of the SOP. In the proposed algorithm there are two key parameters:

- T_{mov}: represents the averaging window length in seconds, on the acquired SOPAS traces. The finite impulse response (FIR) filter in Fig. 5 is in fact a moving average filter, used to smooth the SOPAS time evolution. Thus, at the output of the FIR filter we obtain the smoothed SOPAS samples $\omega_s[k]$. Fig. 6 shows the SOPAS time evolutions, when T_{mov} is set to one second, when no event is generated (in black) and for 10 RF events occurrences, measured through fiber T3. The inset in Fig. 6 shows how the SOP change rate evolves during events with different mechanical intensity, related to the size and weight of the items used to generate them. The relationship between vibrations and SOP variation is first of all non linear, but also it depends on how the vibrations generated by the falling rocks impinge on the underground fibers. This is thus hard to be properly defined, even though it is evident that a higher angular speed is produced by stronger events. In our specific experimental setup, RF is the most intense as it is composed of several rocks, SR is the weakest as it is generated only by a small rock, C is in between as it is generated by a cylinder bigger than the single rock. At the output of the FIR filter we obtain the smoothed SOPAS samples $\omega_s[k]$.
- ω_{th}: is the SOPAS threshold value, in rad/s. If the algorithm detects $\omega_s[k] > \omega_{th}$ an alarm signal is generated.

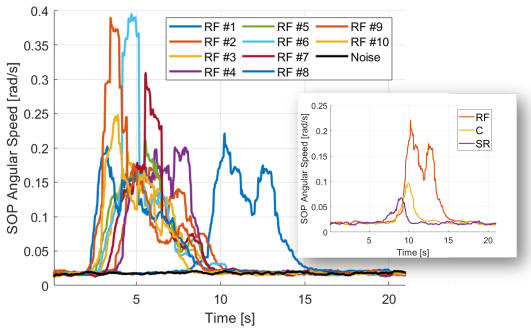

Fig. 6. Ten different runs of RF and one of background noise on fiber T3, represented with different colors and using $T_{mov} = 1$ second, $f_s = 48.83$ kHz. The inset shows an example of SOPAS traces for the three tested events.

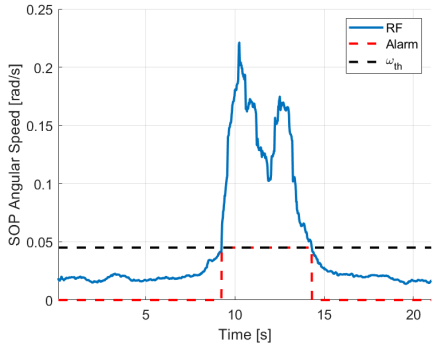

Fig. 7. Rockfalls SOPAS on fiber T3, ω_{th} and alarm signal using $T_{mov} = 1$ second, $f_s = 48.83$ kHz.

As an example, Fig. 7 shows one SOPAS trace for a single RF event measured on fiber T3, compared to a threshold ω_{th}=0.045 rad/s. The two-state alarm signal is also represented in red. In a real world scenario, it could trigger a traffic light turning red and/or send a message to a remote emergency control room. As any "binary" alarm system, its performance depends on the probability of the following three situations:

- **Missed detection (MD)**: an anomalous event is not detected (threshold ω_{th} is thus too high).
- **False alarm (FA)**: no event takes place, but the system generates an alarm (threshold is too low).
- **Correct detection (CD)**: events are accurately detected in the SOPAS time evolution, with no FAs or MDs.

Ideally, our system should always be in the CD condition. The probability for the other two conditions to occur is minimized by appropriately choosing T_{mov} and ω_{th}. In Fig. 8, the same SOPAS evolution of a RF event is reported for three different T_{mov} values. For increasing values of the averaging window, the oscillations in the original SOPAS evolution reduce, making the algorithm more robust. Nevertheless, peaks are also lower, requiring a lower threshold to be selected. If the threshold value is set too high without accounting for this

This article has been accepted for publication in IEEE Photonics Journal. This is the author's version which has not been fully edited and content may change prior to final publication. Citation information: DOI 10.1109/JPHOT.2023.3281670

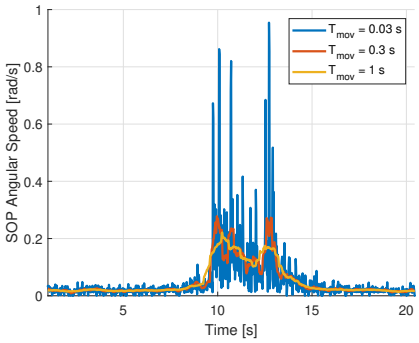

Fig. 8. SOPAS time evolution of a RF event generated on T3 for different T_{mov} values, using $f_s = 48.83$ kHz.

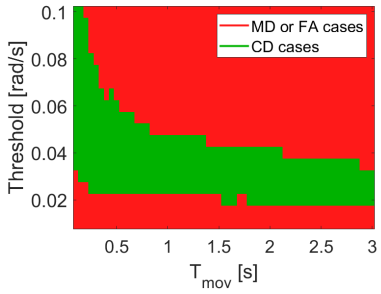

Fig. 9. Detection map for 10 SR events generated on T3. $f_s = 48.83$ kHz.

effect, MD cases are likely to happen. On the other hand, a very low value of T_{mov} could enhance the noise oscillations and, if the threshold is set too low, trigger the alarm generating FAs. The choice of T_{mov} is also paramount since it is the parameter that determines the speed of reaction of our system. In fact, to a first approximation, the system latency is directly proportional to T_{mov} (plus the polarimenter and DSP internal delay in data transfer). These considerations show that the setting of the pair of parameters T_{mov} and ω_{th} is key for the correct operation of our setup.

IV. Experimental Results and Assessment of System Performance

A. SOP post-processing approach for parameter setting

In this Subsection we focus on selecting, for each fiber in our setup, the optimal parameters of the detection algorithm. To perform this analysis, for each fiber we have generated 10 RF, 10 C, 10 SR events, and also acquired 3 steady state traces. These traces show a "noisy" random SOPAS evolution, and are essential in assessing the probability of false alarms. In total, 33 events per fiber have been generated, that is 99 for the whole set of T fibers. The sampling frequency is set to 48.83 kHz and the acquisition time is 21.5 seconds.

The output of the post-processing analysis is a two-dimensional color map showing, for each parameter pair $[T_{mov}, \omega_{th}]$, whether or not the algorithm works in CD mode. We call these "detection maps" (see for instance Fig. 9). To generate these maps we acquired the 13 SOPAS traces per fiber (10 traces for the event and 3 traces for the steady state) and averaged them using several T_{mov} values, from 0.1 seconds to 3 seconds, in order to obtain the smoothing effect

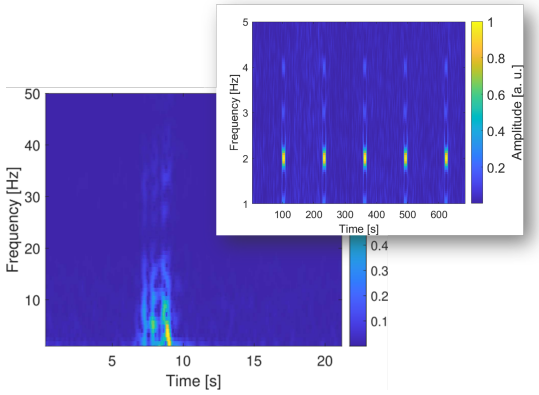

Fig. 10. SOPAS spectrogam of a SR event in linear, normalized scale. The inset shows the SOPAS spectrogram when periodically inducing a 2 Hz sinusoidal vibration on the fiber.

reported in Fig. 8. The resulting averaged SOPAS traces are then compared against different thresholds ω_{th}, and the results obtained as follows:

- if the averaged SOPAS for all 10 events has at least one sample above threshold and all the samples of the averaged steady-state event below threshold we are in a CD condition.
- if at least one sample of the averaged steady-state event is above threshold, we are in a FA condition.
- if all the samples of the averaged SOPAS evolution for at least one of the 10 events are below threshold we are in MD condition.

In Fig. 9 an example of detection map for the single rock events over fiber T3 is reported using the following color convention: green color if all 10 events have generated CD, red color if there was at least one FA (ω_{th} too low) or MD (ω_{th} too high). Thus, all parameter pairs falling in the green area yield a correct working condition for the 10 events on the specific fiber.

After this preliminary investigation on the T_{mov} and ω_{th} parameters, we focus on trying to reduce the sampling frequency of the SOPAS evolution. We started by observing the typical frequency content of a SOPAS trace during an anomalous event: an example is given in Fig. 10 as time-frequency spectrogram. It is evident that most of the spectral content is below 10 Hz, as it is typical for these kinds of mechanical vibration events on the terrain [26], [27]. Although in our case we work on a reduced scale experimental model, this frequency range is in line with those reported in other paper dealing with similar topics, such as [28] and [29]. The inset of Figure 10 shows how a short (about 1 m) span of fiber reacts to mechanical vibrations in a controlled laboratory environment. We induced 2 Hz sinusoidal oscillation on the fiber, for 30 seconds, once every two minutes by means of a vibration generator. The result is shown again as spectrogram: the 2 Hz frequency component and also its higher and lower harmonics are perfectly visible in the spectrum of the SOPAS, indicating that the frequency components of the mechanical stress are transferred to the SOP variation. However, the way this transfer occurs is not trivial, and depends on factors such

This article has been accepted for publication in IEEE Photonics Journal. This is the author's version which has not been fully edited and
content may change prior to final publication. Citation information: DOI 10.1109/JPHOT.2023.3281670

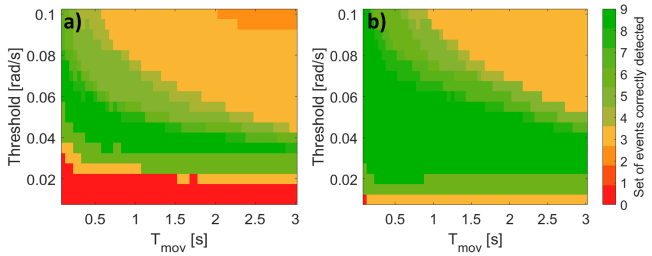

Fig. 11. Detection map considering all T fibers and all realizations of the 3 events a) with f_s = 48.83 kHz and b) with f_s = 95.4 Hz.

as length of the fiber, distance of the event from it, and intensity of the stress. Thanks to this observation, we reduced the sampling frequency down to $f_s = 95.4$ Hz, which happens to be the lowest one enabled by the polarimeter: this is in itself an interesting result, since it goes in the direction of reducing the computational effort. For instance, $f_s = 95.4$ Hz would allow the use of extremely low cost analog-to-digital converters (ADC) and DSP processing boards. Regarding the polarimeter, in our setup we use a quite expensive (about 12000 euros) "high end" device which potentially allows extremely high sampling frequency, but there are lower cost instruments (around 5000 euros) on the market with sampling rates in the 100 sample/s range. Besides this techno-economic consideration, when reducing f_s we also observed in all cases an enhanced operational space in the aforementioned color map, due to the fact that the used polarimeter has a decreasing noise level for decreasing f_s, as demonstrated in the following.

The map shown in Fig. 9 refers to a single fiber but we extended the study further to have a global picture of the situation on all the three T fibers and three events repeated ten times (thus 90 cases in total). Fig. 11a and Fig. 11b summarize the experimental results showing the intersection between the detection maps, respectively with $f_s = 48.83$ kHz and with $f_s = 95.4$ Hz. The dark green area is the region where the algorithm is able to correctly detect all of the 90 events per fiber (ten repetitions of the C, SR and RF events for each of the T fiber at three different depths). One unit on the colorbar corresponds to one set of ten SR, RF or C events that, for a single fiber, has been correctly detected. A set is not correctly detected if at least one of the ten events in the set is not correctly detected. In this case the set does not add to the colorbar count. A clear advantage can be observed when using the lowest sampling frequency ($f_s = 95.4$ Hz), as the dark green area is much larger in Fig. 11b (it represents the 12% of the whole parameter space in Fig. 11a, whereas it represents about the 40% of the total in Fig. 11b, a threefold increase).

The same analysis has been performed also for the other application, i.e. for the rockfall barriers, keeping f_s to the optimal value of 95.4 Hz. In this case 20 SR events were generated by launching one small stone 20 times. The detection maps are shown in Fig. 12. Maps 12a, 12b, 12c and 12d refer to RB1, RB2, RB3 and RB4 configurations, respectively. The ability of the system to detect single rocks when applied to the barrier is even greater: the green area covers more than 70% of the entire parameters space in all cases, except for

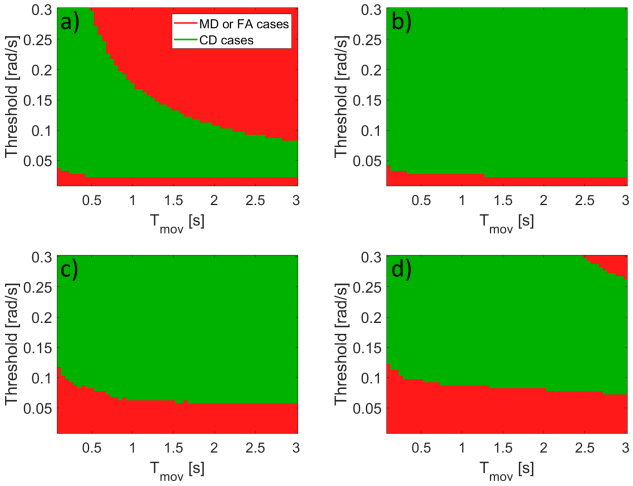

Fig. 12. Detection maps of a) RB1, b) RB2, c) RB3 and d) RB4 fibers configurations for the emulation of a rockfall barrier, with f_s = 95.4 Hz.

configuration RB1 (Fig. 12a), where it is just the 46%. The best performing configuration is the RB2, with a green area covering the 94% of the map, because, as shown in Fig. 4, in order to create the loops, two portions of fibers are almost overlapping at the center of the barrier, where the stone is more likely to hit, enhancing the effect on the SOPAS.

B. Long term measurement

In this Subsection, we apply the algorithm in Fig. 5 to continuously monitor over long time windows (up to tens of minutes) and for many anomalous events. This approach was used to test the post-processing algorithm introduced in the previous sections in a more realistic scenario, where the events occur sequentially at time instants unknown a priori. The parameters set for the acquisitions are $f_s = 95.4$ Hz and $t_{tot} = 22.9$ minutes. The events generated are: three RF, one SR and one C, and are shown in Fig. 13. Specifically, they were generated in the following order during the acquisition: RF, SR, RF, C, and lastly RF again. Fig. 13 shows the three detection scenarios: false alarm in Fig. 13a ($T_{mov} = 0.3$ seconds, $\omega_{th} = 0.015$ rad/s); correct detection in Fig. 13b ($T_{mov} = 1$ second, $\omega_{th} = 0.06$ rad/s) and Fig. 13c ($T_{mov} = 2$ seconds, $\omega_{th} = 0.06$ rad/s); missed detection in Fig. 13d ($T_{mov} = 3$ seconds, $\omega_{th} = 0.06$ rad/s). The blue line represents the smoothed SOPAS, the black dashed line represents the threshold value, while the red dots highlight the time instants in which the alarm signal would be triggered. These graphs confirm that, by appropriately choosing the parameters pair ω_{th} and T_{mov} the algorithm can be made to work according to the detection map of Fig. 11b. For example, Fig. 13a shows that by picking $T_{mov} = 0.3$ seconds and $\omega_{th} = 0.015$ rad/s, we get FA, which is predicted by the detection map. This is confirmed also for the other three cases. For instance, when we pick a parameters pair inside the green area of Fig. 11b the algorithm correctly detects all the different events (see Fig. 13b and Fig. 13c). In a real field installation, we envision that a higher layer algorithm can adaptively set these two parameters, and in particular the threshold ω_{th}.

This article has been accepted for publication in IEEE Photonics Journal. This is the author's version which has not been fully edited and
content may change prior to final publication. Citation information: DOI 10.1109/JPHOT.2023.3281670

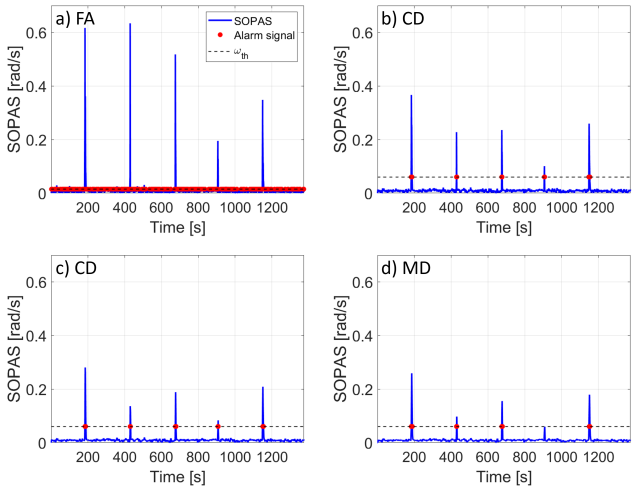

Fig. 13. Long term algorithm simulation in a) FA ($T_{mov} = 0.3$ seconds, $\omega_{th} = 0.015$ rad/s), b) CD ($T_{mov} = 1$ second, $\omega_{th} = 0.06$ rad/s), c) CD ($T_{mov} = 2$ seconds, $\omega_{th} = 0.06$ rad/s) and d) MD ($T_{mov} = 3$ seconds, $\omega_{th} = 0.06$ rad/s) conditions, over T3 fiber. The legend in a) applies to b), c) and d) as well.

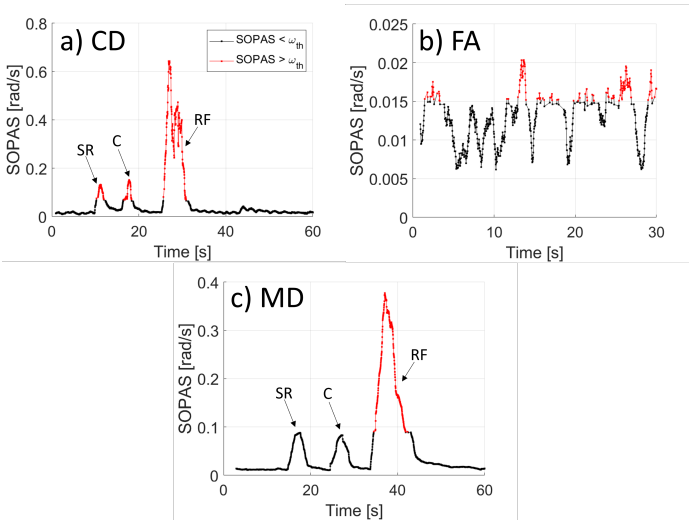

Fig. 14. a) occurrences of SR, C and RF events in CD conditions ($T_{mov} = 0.3$ seconds, $\omega_{th} = 0.07$ rad/s). b) Only noise generating FA ($T_{mov} = 0.3$ seconds, $\omega_{th} = 0.015$ rad/s). c) SR, C and RF events in MD conditions ($T_{mov} = 1$ second, $\omega_{th} = 0.09$ rad/s). All the plots show a real-time acquisition over T3 fiber. Note that the vertical axis has been adapted to enhance visualization. Legend in a) applies to b) and c) too.

C. Real-time processing approach

In this Subsection, we focus on a true real-time application of the algorithm on the same experimental setup (see Fig. 2). The Stokes parameters are now extracted from the polarimeter internal memory and the algorithm was modified to operate in real-time, generating alarms immediately after the detection of anomalous events. Thanks to a sampling frequency smaller than 100 Hz, it was possible to use a simple Matlab script on a standard laptop: to extract the Stokes vector from the device and compute one sample of SOPAS, in the current version, the algorithm introduces a latency of the order of 1 ms.

In our real-time implementation, the SOPAS time evolution is displayed at every sampling instant: each time ω_{th} is exceeded the point on the curve is plot in red and a sound is emitted. We performed several test and show three of them in Fig. 14. The sampling frequency was set to 95.4 Hz, and the parameter pair values were chosen from the map in Fig. 11b, in order to generate CD, FA and MD, and test the consistency of the post-processing results with the real-time approach. The three subfigures in Fig. 14 show:

a) Correct detection (Fig. 14a): parameters were set to $T_{mov} = 0.3$ s and $\omega_{th} = 0.07$ rad/s. A SR, a C and a RF event were correctly detected.
b) False alarm (Fig. 14b): parameters were set to $T_{mov} = 0.3$ s and $\omega_{th} = 0.015$ rad/s. No events were generated in this case, but the threshold was too low and the noise alone triggered the alarm.
c) Missed detection (Fig. 14c): parameters were set to $T_{mov} = 1$ s and $\omega_{th} = 0.09$ rad/s. A SR, a C and a RF event were generated, but only the RF was detected.

Fig. 14 shows that also in a real-time application, if the parameters pair is set appropriately, the algorithm works correctly, and the performance is consistent with that estimated in post-processing through the detection maps.

V. Discussions

Compared to a real installation (e.g. on a mountain gully), the SOPAS traces obtained on the small-scale model are less noisy in the steady state condition since the fiber is shorter, but the anomalous events that we were able to generate are weaker than in a real mountain environment. We envision that f_s around 100 Hz and T_{mov} of a few seconds, could approximately remain the same also in a real environment. In fact, the chosen f_s allows to detect anomalies whose spectral content is limited to a few tens of Hz, as for the events of interest in our case. Moreover, we experimentally verified that the tested averaging window values work for a whole range of weak and intense events. The setting of ω_{th} is the most crucial, since this SOPAS threshold at which real anomalous events should trigger an alarm, depends on many factors, such as: 1) depth at which the fiber are deployed underground; 2) position of the fibers (for instance, in the center of a gully or slighlty on its side); 3) strength of the anomalous events; 4) characteristics of the SOPAS noise in the steady state; 5) composition of the debris material; 6) the flow dynamics - smooth or surge type flows. Moreover, landslides and debris flows are often erosive phenomena. Erosion, entrainment and deposition processes result in crucial change of local material compositions, properties and flow dynamics, including the flow depth, speed and mobility [30]. For these complex, but realistic situations, the performances of the proposed system should also be checked. In a real installation, the probability of false alarms can be high since spurious events (animals or people crossing the fibers, for example) would commonly occur and a threshold based algorithm, although adaptive, would likely sense them. This can be mitigated by monitoring in parallel more than one fiber by means, for example, of an optical switch, and activate the alarm only if ω_{th} is exceeded on the SOP variation on all of them. In fact, anomalous

TABLE I
COMPARISON BETWEEN THE PROPOSED MONITORING SYSTEM AND EXISTING SOLUTIONS [31]–[37].

Method	Characteristics	Pros	Cons
Geophones, accelerometers, infrasonic sensors and seismometers	Measures the vibrations or sound waves associated to the debris propagation	Easy and safe installation	Limited reliability/accuracy, requires supply on site, calibration and interpretation
Ultrasonic and doppler radar sensors	Measures the level variations on specific point along a channel/gully	High reliability/accuracy	Applicable for narrow channels only, need to hang sensors over the channel, high risk of damages during the event, requires supply on site, visual impact
Wire, pendulum and impact sensors (i.e. electromechanical systems)	Installed on specific check points (trigger lines), detects the arrival of debris/snow masses	Reduced costs, high reliability/accuracy	High risk of damages during the event, need to hang sensors over the channel, requires supply on site, environment impact
Photocells and high resolution infrared cameras (i.e. optical systems)	Manual or automatic identification of the debris flows/avalanches transit	Visual acquisition	Limited reliability/accuracy, limited visibility in case of bad weather and night, high risk of damages during the event, requires supply and installation on site
Remote doppler radar sensors	Detects the initiation of avalanches on wide areas	Only one measurement point, reduced risk of damages	Very expensive, need of a visible scenario, requires supply at the installation point
Fiber-optic SOP sensing	Monitors ground vibrations related to debris flow propagation along channels	Reduced risk of damages, limited cost, high reliability/accuracy, supply required only at the polarimeter, no visual impact	Need to bury the fiber along the slope

extreme events are usually spatially diffused, and would surely be detected by more than one fiber, whereas spurious events are usually localized and would be sensed by only one of them. Machine learning algorithms [38]–[40] can also be used to distinguish between steady state and hazardous conditions, and can also enable event type classification. Regarding viability and cost of a real installation, we have recently installed a monitoring system like the proposed one in the Valle d'Aosta region, Italy. Here, an optical fiber bundle, containing 24 fibers, runs for a few hundred meters along a mountain road, and is then buried inside a corrugated hose for extra 100 m, along the gully. Access to the fibers is possible through manholes placed every 100 m. The cost associated to the installation can be high, but can be mitigated. Firstly, optical fibers are rather inexpensive: one cable containing around 50 fibers can cost around 1 EUR/m. Moreover, many roads nowadays have already been outfitted with data-carrying optical fiber cables and thus the cost associated with the excavation can, in some cases, be reduced or disregarded. Furthermore, we are working on a system configuration which allows to exploit different fibers contained in the same cable, to monitor different sites by using the same interrogator, equipped with a low cost optical switch. Another cost element is related to the need to replace the damaged fiber in the event of a particularly strong catastrophic rockfall phenomenon. In a practical installation, we envision the interrogator to be placed in a convenient location several km far from the mountain slope. Potential damages would occur only on the portion of the fiber installed in the "dangerous" area, which would be only a few hundred meters long. The breaking point could be determined by exploiting an optical time domain reflectometer (OTDR), which can pinpoint any loss on the cable with cm accuracy. Moreover, such a catastrophic event causing a cable break, would for sure be sensed by our system, that would generate the alarm and fulfill its duty before fiber replacement can take place. A system with these characteristics could really represent a valid alternative to current early warning and detection systems available on the market. A comparison of pros and cons is summarized in Table I with respect to most common sensors. The proposed system combines the high accuracy with the robustness and durability required in a mountain environment, at a comparable cost with the cheapest alternatives. It also avoids the need of installation of sustaining systems on site, as well as of electric supply along gullies where cable electricity is usually not available and photovoltaic cells may be harmed by bad exposure. The system may also allow to monitoring different slopes at the same time, as well as large areas, with a single acquisition system. Another suitable alternative in this case would be the remote radar doppler which, however, would require full and clear visibility of the scenario from the installation point and would be much more expensive in the end.

VI. CONCLUSIONS

In this work we proposed and demonstrated a fiber-based mountain anomalous event alarm system, completely relying on polarization variation sensing. Dangerous events have been emulated over a scale model of a mountain slope, where different fiber configurations have been installed. The alarm algorithm is low on complexity and based on SOPAS computation, smoothing operation and threshold comparison. Its performances strongly depend on T_{mov}, ω_{th} and f_s: detection maps have been generated to appropriately set the first two parameters and avoid FA and MD, while we proved that the

optimal choice of sampling frequency is the lowest available one, 95.4 Hz. By setting $f_s = 95.4$ Hz, the detection map shows a clear increase of the operational space, compared to higher sampling frequencies. It has been successfully tested that if the parameters pair is chosen appropriately from the map, correct detection of the dangerous events can always be obtained, even in a real-time scenario. Moreover, one of the main results of this work is having optimized performances setting a low f_s, which opens to the possibility of using less costly devices. The proposed system is then reliable, simple and requires a low cost interrogator.

REFERENCES

[1] B. Culshaw and A. Kersey, "Fiber-Optic Sensing: A Historical Perspective," *Journal of Lightwave Technology*, vol. 26, no. 9, pp. 1064–1078, 2008.

[2] S. Aiassa, F. Antolini, M. Barla, A. Insana, R. Gaudino, G. Rizzelli Martella, and S. Pellegrini, "A new real-time debris flow and avalanches detection system based on optical fiber sensing," in *Proceedings of the 8th International Conference on Debris Flow Hazard Mitigation*, 2023.

[3] A. H. Hartog, *An Introduction to Distributed Optical Fibre Sensors*. CRC Press, 2017.

[4] G. Ball, W. Morey, and P. Cheo, "Single and multipoint fiber-laser sensors," *IEEE Photonics Technology Letters*, vol. 5, no. 2, pp. 267–270, 1993.

[5] A. Alavie, S. Karr, A. Othonos, and R. Measures, "A multiplexed Bragg grating fiber laser sensor system," *IEEE Photonics Technology Letters*, vol. 5, no. 9, pp. 1112–1114, 1993.

[6] I. Di Luch, P. Boffi, M. Ferrario, G. Rizzelli, R. Gaudino, and M. Martinelli, "Vibration Sensing for Deployed Metropolitan Fiber Infrastructure," *Journal of Lightwave Technology*, vol. 39, no. 4, pp. 1204–1211, 2021.

[7] I. Di Luch, M. Ferrario, G. Rizzelli, R. Gaudino, and P. Boffi, "Vibration Sensing for Deployed Metropolitan Fiber Infrastructures," in *Proceedings of 2020 Optical Fiber Communications Conference and Exhibition*, 2020.

[8] I. Di Luch, M. Ferrario, P. Boffi, G. Rizzelli, H. Wang, and R. Gaudino, "Demonstration of structural vibration sensing in a deployed PON infrastructure," in *Proceedings of the 45th European Conference on Optical Communication (ECOC 2019)*, 2019, pp. 1–3.

[9] M. Mergili, M. Jaboyedoff, J. Pullarello, and S. P. Pudasaini, "Back calculation of the 2017 piz cengalo–bondo landslide cascade with r.avaflow: what we can do and what we can learn," *Natural Hazards and Earth System Sciences*, vol. 20, no. 2, pp. 505–520, 2020.

[10] S. P. Pudasaini and M. Mergili, "A multi-phase mass flow model," *Journal of Geophysical Research: Earth Surface*, vol. 124, no. 12, pp. 2920–2942, 2019.

[11] R. Kostynick, H. Matinpour, S. Pradeep, S. Haber, A. Sauret, E. Meiburg, T. Dunne, P. Arratia, and D. Jerolmack, "Rheology of debris flow materials is controlled by the distance from jamming," *In Proceedings of the National Academy of Sciences*, vol. 119, no. 44, 2022.

[12] M. Hürlimann, V. Coviello, C. Bel, X. Guo, M. Berti, C. Graf, J. Hbl, S. Miyata, J. B. Smith, and H.-Y. Yin, "Debris-flow monitoring and warning: Review and examples," *Earth-Science Reviews*, vol. 199, p. 102981, 2019.

[13] L. Zan, G. Latini, E. Piscina, G. Polloni, and P. Baldelli, "Landslides early warning monitoring system," in *Proceedings of the IEEE International Geoscience and Remote Sensing Symposium*, vol. 1, 2002, pp. 188–190.

[14] L. Schenato, "A Review of Distributed Fibre Optic Sensors for Geo-Hydrological Applications," *Applied Sciences*, vol. 7, no. 9, 2017.

[15] Y. Yan, H. Zheng, A. P. T. Lau, C. Guo, and C. Lu, "Unidirectional Ultra-Long Distributed Optical Fiber Sensor," *IEEE Photonics Journal*, vol. 13, no. 4, pp. 1–7, 2021.

[16] Y. Koyamada, M. Imahama, K. Kubota, and K. Hogari, "Fiber-Optic Distributed Strain and Temperature Sensing With Very High Measurand Resolution Over Long Range Using Coherent OTDR," *Journal of Lightwave Technology*, vol. 27, no. 9, pp. 1142–1146, 2009.

[17] L. Schenato, A. Pasuto, A. Galtarossa, and L. Palmieri, "On the use of OFDR for high-spatial resolution strain measurements in mechanical and geotechnical engineering," in *Proceedings of the 2018 IEEE International Instrumentation and Measurement Technology Conference (I2MTC)*, 2018, pp. 1–6.

[18] S. Ramo, J. R. Whinnery, and T. V. Duzer, *Fields and Waves in Communication Electronics*. Wiley, 2014.

[19] M. Bass, C. DeCusatis, J. Enoch, V. Lakshminarayanan, G. Li, C. MacDonald, V. Mahajan, and E. Van Stryland, *Handbook of Optics, Volume 1*. McGraw-Hill, 2010.

[20] H. Kogelnik and P. J. Winzer, "Modal birefringence in weakly guiding fibers," *Journal of Lightwave Technology*, vol. 30, no. 14, pp. 2240–2245, 2012.

[21] K. Okamoto, *Fundamentals of Optical Waveguides*. Elsevier Science, 2006.

[22] FOSCO. What is birefringence and beat length? [Online]. Available: https://www.fiberoptics4sale.com/blogs/archive-posts/95042886-what-is-birefringence-and-beat-length

[23] M. Piantini, F. Gimbert, E. Korkolis, R. Rousseau, H. Bellot, and A. Recking, "Solid Concentration as a Main Proxy for Basal Force Fluctuations Generated by Highly Concentrated Sediment Flows," *Geophysical Research Letters*, vol. 50, no. 1, p. e2022GL100345, 2023.

[24] S. Li, J. Ma, and J. Hu, "Rockfall hazard alarm strategy based on FBG smart passive net structure," *Photonic Sensors*, vol. 5, no. 9, pp. 19–23, 2015.

[25] Y. Yan, T. Li, J. Liu, W. Wang, and Q. Su, "Monitoring and early warning method for a rockfall along railways based on vibration signal characteristics," *Scientific Reports*, vol. 9, p. 6606, 2019.

[26] M. Farin, V. C. Tsai, M. P. Lamb, and K. E. Allstadt, "A physical model of the high-frequency seismic signal generated by debris flows," *Earth Surface Processes and Landforms*, vol. 44, no. 13, pp. 2529–2543, 2019.

[27] A. Mecozzi, C. Antonelli, M. Mazur, N. Fontaine, H. Chen, L. Dallachiesa, and R. Ryf, "Use of optical coherent detection for environmental sensing," in *Proceedings of 2022 European Conference on Optical Communication (ECOC)*, 2022, pp. 1–4.

[28] M. Cantono, J. C. Castellanos, V. Kamalov, A. Mecozzi, R. Muller, S. Yin, and Z. Zhan, "Seismic Sensing in Submarine Fiber Cables," in *Proceedings of 2021 European Conference on Optical Communication (ECOC)*, 2021, pp. 1–3.

[29] A. Mecozzi, M. Cantono, J. C. Castellanos, V. Kamalov, R. Muller, and Z. Zhan, "Polarization sensing using submarine optical cables," *Optica*, vol. 8, no. 6, pp. 788–795, Jun 2021.

[30] S. P. Pudasaini and M. Krautblatter, "The mechanics of landslide mobility with erosion," *Nature Communications*, vol. 12, 2021.

[31] K. Takahashi, D. Mecatti, D. Dei, M. Matsumoto, and M. Sato, "Landslide observation by ground-based SAR interferometry," in *Proceedings of 2012 IEEE International Geoscience and Remote Sensing Symposium*, 2012, pp. 6887–6890.

[32] A. Martinez-Vazquez and J. Fortuny-Guasch, "A GB-SAR Processor for Snow Avalanche Identification," *IEEE Transactions on Geoscience and Remote Sensing*, vol. 46, no. 11, pp. 3948–3956, 2008.

[33] J. Aaron, R. Spielmann, B. W. McArdell, and C. Graf, "High-frequency 3d lidar measurements of a debris flow: A novel method to investigate the dynamics of full-scale events in the field," *Geophysical Research Letters*, vol. 50, no. 5, 2023.

[34] M. V. Ramesh and N. Vasudevan, "The deployment of deep-earth sensor probes for landslide detection," *Landslides*, vol. 9, no. 4, pp. 457–474, 2012.

[35] C. Abanc, M. Hürlimann, B. Fritschi, C. Graf, and J. Moya, "Transformation of ground vibration signal for debris-flow monitoring and detection in alarm systems," *Sensors*, vol. 12, no. 4, pp. 4870–4891, 2012.

[36] M. Arattano and L. Marchi, "Systems and Sensors for Debris-flow Monitoring and Warning," *Sensors*, vol. 8, no. 4, pp. 2436–2452, 2008.

[37] S.-C. Wei and K.-F. Liu, "Automatic debris flow detection using geophones," *Landslides*, vol. 17, no. 2, pp. 349–359, 2020.

[38] P. D. Hernndez, J. A. Ramrez, and M. A. Soto, "Improving Earthquake Detection in Fibre-Optic Distributed Acoustic Sensors Using Deep-Learning and Hybrid Datasets," in *Proceedings of 2022 European Conference on Optical Communication (ECOC)*, 2022, pp. 1–4.

[39] J. Ye, Y. Kurashima, T. Kobayashi, H. Tsuda, T. Takahara, and W. Sakurai, "An Efficient In-Situ Debris Flow Monitoring System over a Wireless Accelerometer Network," *Remote Sensing*, vol. 11, no. 13, 2019.

[40] D. Gong, L. Liu, V. Le, B. Saha, M. R. Mansour, S. Venkatesh, and A. Van Den Hengel, "Memorizing Normality to Detect Anomaly: Memory-Augmented Deep Autoencoder for Unsupervised Anomaly Detection," in *Proceedings of 2019 IEEE/CVF International Conference on Computer Vision (ICCV)*, 2019, pp. 1705–1714.